Available online at www.sciencedirect.com

ScienceDirect

Scripta Materialia 70 (2014) 51–54

Scripta MATERIALIA

www.elsevier.com/locate/scriptamat

Temporal evolution of the γ(fcc)/γ′($L1_2$) interfacial width in binary Ni–Al alloys

Elizaveta Y. Plotnikov,[a] Zugang Mao,[a] Ronald D. Noebe[b] and David N. Seidman[a,c,*]

[a]*Northwestern University, Department of Materials Science and Engineering, Evanston, IL 60208-3108, USA*
[b]*NASA Glenn Research Center, 21000 Brookpark Rd, Cleveland, OH 44135, USA*
[c]*Northwestern University Center for Atom-Probe Tomography, Evanston, IL 60208-3018, USA*

Received 11 July 2013; revised 12 September 2013; accepted 16 September 2013
Available online 23 September 2013

The temporal evolution of γ′($L1_2$ structure) precipitates is studied in Ni–12.5 at.% Al and Ni–13.4 at.% Al alloys, aged at 823 and 873 K, utilizing three-dimensional atom-probe tomography. The values of the interfacial widths, $\delta(t)$s, between the γ(face-centered cubic) and γ′ phases are calculated utilizing proximity histograms. It is demonstrated that $\delta(t)$ decreases continuously with increasing aging time for both Ni–Al alloys: that is, the $\delta(t)$s decrease with increasing mean precipitate radius, $\langle R(t)\rangle$. The ratio $\frac{\delta(t)}{\langle R(t)\rangle}$ decreases, to first order, as $\langle R(t)\rangle^{-1}$.

Keywords: Atom-probe tomography; Nickel–aluminum alloys; Interfacial width; Vacancy-mediated lattice kinetic Monte Carlo simulations

Commercial Ni-based superalloys are utilized for single-crystal turbine blades in commercial and military aircraft jet engines and land-based natural-gas turbine engines due to their high strength, creep, oxidation and corrosion resistance, and toughness at elevated temperatures [1–3]. These alloys are precipitation strengthened by coherent ordered $Ni_3Al(L1_2)$ precipitates (γ′ phase) within a face-centered cubic (fcc) Ni-rich matrix (γ phase) [4,5]. The coarsening rate of γ′ precipitates in Ni-based superalloys is dependent on the interfacial Gibbs free energy, $\sigma^{\gamma/\gamma'}$, between the γ(fcc) and γ′($L1_2$) phases [6–14] as well as the diffusivities of Ni, Al and any additional alloying elements. Lifshitz and Slyozov [15] and Wagner [16] (LSW) derived a model for precipitate coarsening in binary alloys, assuming spherical precipitates, an atomically sharp interface and a constant precipitate composition, forming a vanishingly small volume fraction at all times. The LSW model predicts that, in the stationary-state coarsening regime, the mean precipitate radius, $\langle R(t)\rangle$, is proportional to $t^{1/3}$ This temporal dependence has been found experimentally for several Ni-based alloys [17–28]. Since the advent of atom-probe tomography (APT), it is acknowledged that a coherent precipitate is nothing but a region of the lattice where the concentration and degree of order differ strongly from what it is found in the matrix, with a progressive change between the two regions [21,24,29–31]. The link between models with a diffuse and a sharp interface has been established by Cahn and Hilliard [32] based on classical thermodynamics, and, at least formally, by Martin [33] for kinetics. Recently, the potential effect of interfacial thickness, $\delta(t)$, on the coarsening rate has been addressed: an ansatz was made for $\delta(t)$ which posits that $\delta(t)$ increases as $\langle R(t)\rangle^n$, where $n = m + 2$ and $0 \leqslant m \leqslant 1$ [14,34]. It is, therefore, of great interest to determine experimentally, utilizing APT, how the value of $\delta(t)$, as measured by its compositional variation across the interface between the two phases, varies with increasing aging time for Ni–Al alloys. Binary Ni–Al systems are important as they form the basis of commercial superalloys, which can contain 10 plus alloying elements [1–3,35,36].

Two binary Ni–Al alloys were analyzed in this study: Ni–12.5 at.% Al aged at 823 K, and Ni–12.5 at.% Al and Ni–13.4 at.% Al both aged at 873 K. High-purity Ni and Al were induction-melted under flowing Ar and chill cast in a 19 mm diameter copper mold to form coarse-grained polycrystalline master ingots. Samples from the master ingots were subjected to a three-stage heat treatment: (1) homogenization in the γ(fcc) phase field at 1573 K for 20 h; (2) a solution treatment in the γ(fcc) phase field

* Corresponding author at: Northwestern University, Department of Materials Science and Engineering, Evanston, IL 60208-3108, USA. Tel.: +1 847 491 4391; e-mail: d-seidman@northwestern.edu

1359-6462/$ - see front matter © 2013 Acta Materialia Inc. Published by Elsevier Ltd. All rights reserved.
http://dx.doi.org/10.1016/j.scriptamat.2013.09.016

at 1223 K for 3 h, followed by a direct drop quench into water; and (3) isothermal aging for times ranging from 5 min to 4096 h, followed by an ice-brine water quench. Local-electrode atom-probe (LEAP) tomography, or atom-probe tomography (APT), samples were prepared by cutting the aged ingots into 1 cm long rods with 0.3×0.3 mm^2 cross-sections [37]. The rods were electropolished at room temperature using 10% perchloric acid in acetic acid for coarse polishing and 2% perchloric acid in 2-butoxyethanol for fine polishing: electropolishing was performed at 8–20 V dc [38]. APT analyses were performed using ultraviolet (wavelength = 355 nm) picosecond laser pulsing with an energy of 5 pJ per pulse, a pulse repetition rate of 200 kHz, a detection rate of 5%, a specimen base temperature of 35 ± 1 K and an ambient gauge pressure of $<6.7 \times 10^{-8}$ Pa. APT data were analyzed using the program IVAS 3.6 (Cameca, Madison, WI). The three-dimensional (3-D) reconstructions were generated using a volumetric pixel (voxel) size of 1 nm^3 to perform calculations of the elemental concentrations and a delocalization distance of 3.5 nm, over which local fluctuations in elemental concentrations were smoothed [39,40]. The 3-D reconstructions were generated using a voxel size of 1 nm and a delocalization distance of 3.5 nm [39,40]. The γ' precipitates were identified with Ni isoconcentration surfaces using the inflection point methodology [21], and compositional information was extracted using the proximity histogram procedure [39,41]. The volume equivalent radius, R, of each γ' precipitate was calculated using [42]:

$$R = \left(\frac{3n}{4\pi\rho\xi}\right)^{1/3} \tag{1}$$

where n is the total number of atoms enclosed within an isoconcentration surface, ρ is the atomic number density of the γ' phase, 89.4 atoms nm^{-3}, and ξ is the detection efficiency of the two-dimensional microchannel plate (MCP), 50%. The quantity R assumes a spherical morphology for all precipitates; it can, however, be used to compare the dimensions of spherical precipitates at aging times of <100 h with cuboidal precipitates that appear at aging times >100 h, including the transition from spheroids to cuboids. Figure 1 displays $\langle R(t)\rangle$ vs. aging time data for Ni–12.5 at.% Al aged at 873 K. The data were analyzed using a least squares multivariable regression method. $\langle R(t)\rangle$ was found to be proportional to $t^{0.35\pm0.03}$, consistent with the LSW model.

Figure 2 exhibits the concentration profiles of Al for the Ni–12.5 at.% Al and Ni–13.4 at.% Al alloys after 1 h of aging. The $\delta(t)$s were measured by fitting each concentration profile to a spline curve, with the plateaus of the profiles matching the far-field concentrations determined for the γ and γ' phases. A spline fit produces a piecewise-defined function where the distance between each data point in a data set is fit to a cubic interpolation [43]. The horizontal distance between the 10th and 90th percentiles of the concentration difference between the γ and γ' phases was defined to be the $\delta(t)$ of the γ/γ' interfacial region. The spatial resolution of each concentration profile is 0.1 nm, which is smaller than the lattice parameter of Ni_3Al, 0.355 nm [44,45]. The smallest value of $\langle R(t)\rangle$ we measured is 0.84 nm, and a spatial

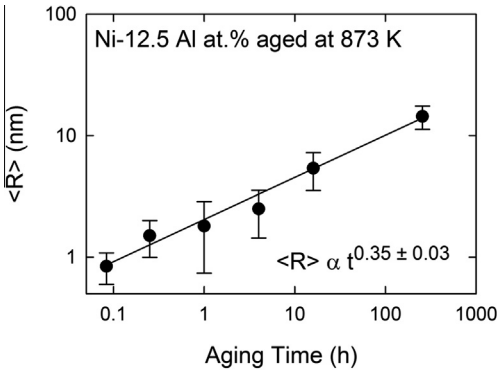

Figure 1. Mean radius, $\langle R(t)\rangle$, vs. aging time for Ni–12.5 at.% Al aged at 873 K, with the error bars indicating plus or minus two standard deviations. $\langle R(t)\rangle$ is found experimentally to vary as $t = 0.35 \pm 0.03$, which is consistent with the LSW model.

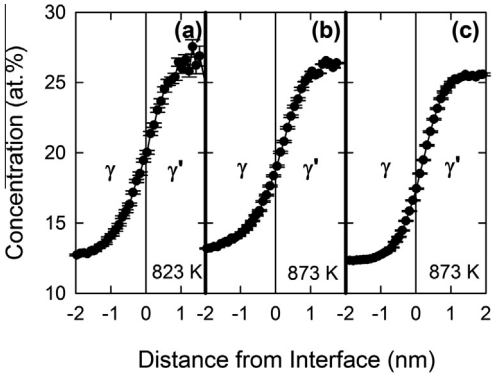

Figure 2. Aluminum concentration profiles across the γ/γ' interface for: (a) Ni–12.5 at.% Al aged at 823 K; (b) Ni–12.5 at.% Al aged at 873 K; and (c) Ni–13.4 at.% Al aged at 873 K. All specimens were aged for 1 h at their indicated aging temperatures. Positive distances are into the γ' precipitates, while negative distances are into the γ matrix. The spatial resolution is 0.1 nm.

resolution of 0.1 nm implies that within the precipitates there are ~230 atoms (115 detected atoms multiplied by two due to the MCP efficiency, 50%). For each data point, the goodness of fit (the coefficient of determination for the entire data set plus the coefficient of determination of the local interfacial region) of the spline function was compared to the goodness of fit for a sigmoidal function, and in each case the spline function produced a better overall fit to the experimental data; this effect was more prominent at earlier aging times.

Each measured $\delta(t)$ (Figure 3) was normalized by its $\langle R(t)\rangle$ value. The resulting normalized widths, $\frac{\delta(t)}{\langle R(t)\rangle}$, (Figure 4), decrease unambiguously with increasing $\langle R(t)\rangle$ by a factor of 10 from $t = 0.25$ to 256 h for two alloys at two temperatures. A multivariable least-squares regression analysis [28] was performed to fit the data to a decaying power-law function:

$$\frac{\delta(t)}{\langle R(t)\rangle} = \psi\langle R(t)\rangle^p \tag{2}$$

by permitting the rate constant, ψ, and the exponent, p, to vary. Table 1 summarizes the values of ψ, p and the coefficient of determination (λ^2) for each fit. For the

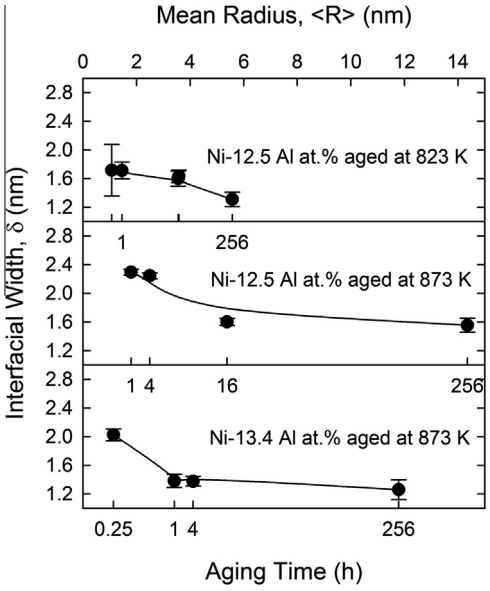

Figure 3. Interfacial width, $\delta(t)$, between the γ and γ' phases as a function of the mean radius, $\langle R(t)\rangle$, of the γ' precipitates. The solid circles show experimental data points with plus or minus two standard deviations.

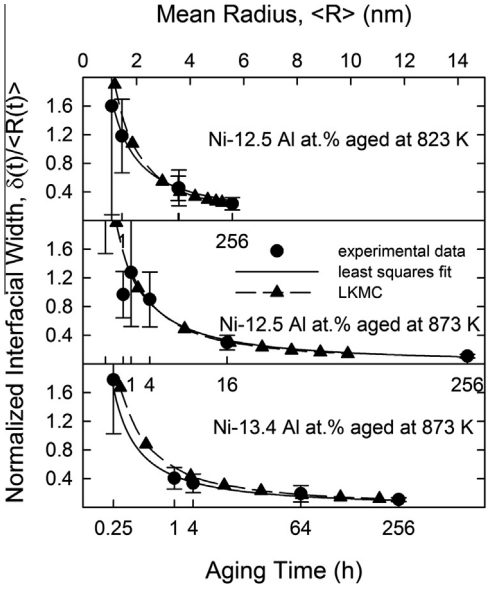

Figure 4. Interfacial width, $\delta(t)$, between the γ and γ' phases normalized by the mean radius, $\langle R(t)\rangle$, of the γ' precipitates as a function of $\langle R(t)\rangle$. The solid circles display experimental atom-probe tomographic data points and the solid triangles indicate vacancy-mediated LKMC simulations results. The experimental data points display plus or minus two standard deviations.

Ni–12.5 at.% Al and Ni–13.4 at.% Al alloys p is found to be negative, consistent with the observed decrease in $\delta(t)$ with increasing $\langle R(t)\rangle$. $\delta(t)$ decreases with time, but it decreases less rapidly than $\langle R(t)\rangle$ increases. Thus, the ratio $\frac{\delta(t)}{\langle R(t)\rangle}$ decreases with increasing time to first order as $\langle R(t)\rangle^{-1}$.

The driving force for phase separation, the supersaturation of Al in the matrix, causes $\delta(t)$ (as measured by its compositional variation across the interface between the two phases) to decrease continuously with increasing aging time, therefore the interfaces are becoming less diffuse as demonstrated experimentally herein. This effect is continuous, as there is not a point during the aging process where $\frac{\delta(t)}{\langle R(t)\rangle}$ increases with increasing $\langle R(t)\rangle$ from 0.25 to 256 h. Moreover, this effect is observed throughout each stage of the phase separation processes: nucleation, nucleation and growth, growth and coarsening, and quasi-stationary coarsening.

In parallel, vacancy-mediated lattice kinetic Monte Carlo (LKMC) simulations were performed for the Ni–12.5 at.% Al and Ni–13.4 at.% Al alloys. The residence-time algorithm employed utilizes a monovacancy, which yields a physically meaningful time for each MC step [46,47]. The kinetic basis of this technique is a thermally activated process involving vacancy mediated diffusion; specifically, a monovacancy exchanging places with a first nearest-neighbor (NN) atom for every jump of an atom. The primitive atomic positions are an array of rhombohedral cells of the fcc lattice and the volume of the simulation box is L^3, where L is 128 in the nucleation regime and 256 in the coarsening regime. A pairwise potential to the fourth nearest-neighbor distance is utilized, where the interactions were determined by first-principles calculations employing VASP. Comparisons between experimental and LKMC results for $\frac{\delta(t)}{\langle R(t)\rangle}$ are displayed in Figure 4 and are in good agreement within experimental errors.

Several models have been proposed to describe phase separation in binary alloys that do not assume a sharp interface, for example, the classic Cahn–Hilliard thermodynamic model [32]. More recently, a kinetic trans-interface-diffusion-controlled (TIDC) model for describing the temporal evolution of binary alloys during aging was presented [34]. Ref. [14] elaborated on the TIDC model by making an ansatz (Eq. (10) in Ref. [14]), which posits that $\delta(t)$ increases with increasing aging time as $\langle R(t)\rangle^n$: $n = m + 2$ where $0 < m < 1$. Additionally, the concentration profiles obtained from our APT dataset results on Ni–Al–Cr alloys [48] were fitted by Ardell to a sigmoid function [14]. In contrast, we find that a spline function provides a better fit to the experimentally acquired concentration profiles for

Table 1. Rate constants, ψ and temporal exponents, p, obtained from the multivariable regression fits of the data displayed in Figure 4, and the coefficient of determination for the fits, λ^2.

Ni–Al alloys aged at different temperatures	Rate constant, Ψ (nm^{-1})	Temporal exponent, p (dimensionless)	Coefficient of determination, λ^2
Ni–12.5 at.% Al aged at 823 K	1.74 ± 0.47	-1.08 ± 0.85	0.981
Ni–12.5 at.% Al aged at 873 K	2.67 ± 0.20	-1.24 ± 0.27	0.994
Ni–13.4 at.% Al aged at 873 K	2.10 ± 0.36	-1.28 ± 0.43	0.991

Ni–Al–Cr alloys [48] than does a sigmoid function. And the value of $\delta(t)$ decreases continuously with aging time for the Ni–12.5 at.% Al and Ni–13.4 at.% Al alloys. Thus, the ansatz for $\delta(t)$ [14] is inconsistent with our experimental observations that the $\delta(t)$s decrease with increasing $\langle R(t)\rangle$ for the aging kinetics of the Ni–12.5 at.% Al and Ni–13.4 at.% Al alloys aged at 823 and 873 K. Similar evidence for a decreasing interfacial width with increasing aging time was found in a Ni–10.0 Al–8.5 Cr–2.0 Ta at.% alloy for specimens aged at 1073 K [49].

In summary, atom-probe tomographic experiments for two Ni–Al alloys demonstrate that the mean radius, $\langle R(t)\rangle$, of $\gamma'(L1_2)$ precipitates increases as $t = 0.35 \pm 0.03$, while the interfacial width, $\delta(t)$, decreases from 0.25 to 256 h for Ni–12.5 at.% Al and Ni–13.4 at.% Al alloys aged at 823 and 873 K. The ratio $\frac{\delta(t)}{\langle R(t)\rangle}$ also decreases, to first order, as $\langle R(t)\rangle^{-1}$ but its value never reaches zero. Additionally, vacancy-mediated LKMC simulations are completely consistent with the experimental APT data, and exhibit the same trend of increasing $\langle R(t)\rangle$ and decreasing $\delta(t)$ in the same range of increasing aging times.

This research was supported by the National Science Foundation, Division of Materials Research (DMR) Grant No. 1207539, Prof. Eric Taleff, grant officer. Atom-probe tomography was performed at the Northwestern University Center for Atom-Probe Tomography (NUCAPT), whose LEAP tomograph was purchased and upgraded with funding from NSF-MRI (DMR-0420532) and ONR-DURIP (N00014-0400798, N00014-0610539, N00014-0910781) grants. Instrumentation at NUCAPT was further upgraded by the Initiative for Sustainability and Energy at Northwestern (ISEN). NUCAPT is a Shared Facility at the Materials Research Center of Northwestern University, partially supported by the National Science Foundation's MRSEC program (DMR-1121262). The authors thank Dr. Georges Martin for his insightful comments and a critical reading of the manuscript.

[1] C.T. Sims, High-Temperature Materials for Aerospace and Industrial Power, Wiley, New York, 1987.
[2] R.C. Reed, The Superalloys: Fundamentals and Applications, Cambridge University Press, Cambridge, 2006.
[3] B.B. Seth, Superalloys – The Utility Gas Turbine Perspective, The Minerals, Metals and Materials Society, Warrendale, PA, 2000.
[4] C.D. Desforges, Rev. Int. Hautes Temp. 14 (1977) 28–45.
[5] Y. Mishima, S. Ochiai, N. Hamao, M. Yodogawa, T. Suzuki, Jpn. Inst. Met. 27 (1986) 656–664.
[6] A.J. Ardell, R.B. Nicholson, Acta Metall. 14 (1966) 1295–1309.
[7] A.J. Ardell, Acta Metall. 16 (1968) 511–516.
[8] D.J. Chellman, A.J. Ardell, Acta Metall. 22 (1974) 577–588.
[9] H. Wendt, P. Haasen, Acta Metall. 31 (1983) 1649–1659.
[10] C. Marsh, H. Chen, Acta Metall. Mater. 38 (1990) 2287–2298.
[11] S.Q. Xiao, P. Haasen, Acta Metall. Mater. 39 (1991) 651–659.
[12] H.A. Calderon, P.W. Voorhees, J.L. Murray, G. Kostorz, Acta Metall. Mater. 42 (1994) 991–1000.
[13] A.J. Ardell, Interface Sci. 3 (1995) 119–125.
[14] A.J. Ardell, J. Mater. Sci. 46 (2011) 4832–4849.
[15] I.M. Lifshitz, V.V. Slyozov, J. Phys. Chem. Solids 19 (1961) 35–50.
[16] C. Wagner, Z. Elektrochem. 65 (1961) 581–591.
[17] C. Schmuck, F. Danoix, P. Caron, A. Hauet, D. Blavette, Appl. Surf. Sci. 94–5 (1996) 273–279.
[18] C. Schmuck, P. Caron, A. Hauet, D. Blavette, Philos. Mag. A 76 (1997) 527–542.
[19] C. Pareige-Schmuck, F. Soisson, D. Blavette, Mater. Sci. Eng. A 250 (1998) 99–103.
[20] C. Pareige, F. Soisson, G. Martin, D. Blavette, Acta Mater. 47 (1999) 1889–1899.
[21] C.K. Sudbrack, D. Isheim, R.D. Noebe, N.S. Jacobson, D.N. Seidman, Microsc. Microanal. 10 (2004) 355–365.
[22] K.E. Yoon, C.K. Sudbrack, R.D. Noebe, D.N. Seidman, Z. Metallkd. 96 (2005) 481–485.
[23] C.K. Sudbrack, R.D. Noebe, D.N. Seidman, Phys. Rev. B 73 (2006) 212101.
[24] C.K. Sudbrack, K.E. Yoon, R.D. Noebe, D.N. Seidman, Acta Mater. 54 (2006) 3199–3210.
[25] C.K. Sudbrack, R.D. Noebe, D.N. Seidman, Acta Mater. 55 (2007) 119–130.
[26] K.E. Yoon, R.D. Noebe, D.N. Seidman, Acta Mater. 55 (2007) 1159–1169.
[27] C.K. Sudbrack, T.D. Ziebell, R.D. Noebe, D.N. Seidman, Acta Mater. 56 (2008) 448–463.
[28] C. Booth-Morrison, J. Weninger, C.K. Sudbrack, Z. Mao, R.D. Noebe, D.N. Seidman, Acta Mater. 56 (2008) 3422–3438.
[29] H. Harada, A. Ishida, Y. Murakami, H.K.D.H. Bhadeshia, M. Yamazaki, Appl. Surf. Sci. 67 (1993) 299–304.
[30] Y. Mishin, Acta Mater. 52 (2004) 1451–1467.
[31] R. Srinivasan, R. Banerjee, J.Y. Hwang, G.B. Viswanathan, J. Tiley, D.M. Dimiduk, H.L. Fraser, Phys. Rev. Lett. 102 (2009) 086101.
[32] J.W. Cahn, J.E. Hilliard, J. Chem. Phys. 28 (1958) 258–267.
[33] G. Martin, Acta Mater. 53 (2005) 2629–2632.
[34] A.J. Ardell, V. Ozolins, Nat. Mater. 4 (2005) 309–316.
[35] J.Y. Hwang, S. Nag, A.R.P. Singh, R. Srinivasan, J. Tiley, H.L. Fraser, R. Banerjee, Scripta Mater. 61 (2009) 92–95.
[36] S. Meher, T. Rojhirunsakool, J.Y. Hwang, S. Nag, J. Tiley, R. Banerjee, Philos. Mag. Lett. 93 (2013) 521–530.
[37] D.N. Seidman, Annu. Rev. Mater. Res. 37 (2007) 127–158.
[38] B.W. Krakauer, D.N. Seidman, Rev. Sci. Instrum. 63 (1992) 4071–4079.
[39] O.C. Hellman, J.B. du Rivage, D.N. Seidman, Ultramicroscopy 95 (2003) 199–205.
[40] O. Hellman, J. Vandenbroucke, J.B. du Rivage, D.N. Seidman, Mater. Sci. Eng. A 327 (2002) 29–33.
[41] O.C. Hellman, J.A. Vandenbroucke, J. Rusing, D. Isheim, D.N. Seidman, Microsc. Microanal. 6 (2000) 437–444.
[42] R.P. Kolli, D.N. Seidman, Microsc. Microanal. 13 (2007) 272–284.
[43] J. Stoer, R. Bulirsch, Introduction to Numerical Analysis, Springer, New York, 2002.
[44] H. Gleiter, E. Hornbogen, Z. Metallkd. 58 (1967) 157–163.
[45] A. Taylor, K.G. Hinton, Jpn. Inst. Met. 81 (1952) 169–180.
[46] Z. Mao, C.K. Sudbrack, K.E. Yoon, G. Martin, D.N. Seidman, Nat. Mater. 6 (2007) 210–216.
[47] Z. Mao, C. Booth-Morrison, C.K. Sudbrack, G. Martin, D.N. Seidman, Acta Mater. 60 (2012) 1871–1888.
[48] C. Booth-Morrison, Y. Zhou, R.D. Noebe, D.N. Seidman, Philos. Mag. 90 (2010) 219–235.
[49] C. Booth-Morrison, R.D. Noebe, D.N. Seidman, Acta Mater. 57 (2009) 909–920.